



Metal sealing mechanism and experimental study of the subsea wellhead connector

Yufang Li¹ · Honglin Zhao¹ · Deguo Wang¹ · Yongbiao Xu¹

Received: 11 June 2019 / Accepted: 30 November 2019 / Published online: 6 December 2019
© The Brazilian Society of Mechanical Sciences and Engineering 2019

Abstract

The subsea wellhead connector is an essential piece of equipment whose successful metal-to-metal sealing capacity is crucial to produce deep-sea oil and gas safely. This paper analyzed the mechanical behavior of the metal seal ring in the subsea wellhead connector under preload and operating conditions while determining the role of contact stress in the theoretical relationship between the seal ring and the structural parameters, as well as working pressure. Theoretical calculations and the finite element method were used to analyze the effects of preload force, contact width, preload compression, and working pressure on contact stress. The results derived from the finite element approach were consistent with those obtained with the theoretical calculation method. Finally, the contact width and preload compression parameters of the metal seal were tested by constructing a test device to evaluate the metal seal of the subsea wellhead connector. The relationship between the preload force, contact width, and preload compression was analyzed, and the maximum sealing pressure under different preload forces was investigated. The results verified the accuracy of the theoretical and finite element calculations. This paper proposed the theoretical calculation method for designing and analyzing the metal seal of the subsea wellhead connector.

Keywords Subsea wellhead connector · Metal seal ring · Sealing mechanism · Sealing experiment · Preload force

1 Introduction

The subsea production system is vital in deepwater oil and gas exploration. It is mainly composed of a subsea tree, subsea wellhead, subsea manifold, subsea wellhead connector, and subsea pipeline [1, 2]. The subsea wellhead connector is essential in the subsea well control connection. This connector is usually installed at the bottom of the subsea blowout preventer and the subsea tree and is used to rapidly connect the subsea tree and the subsea wellhead, as well as the

subsea blowout preventer and subsea wellhead. The subsea wellhead connector creates a pressure barrier between the subsea well control equipment to prevent oil and gas leakage [3].

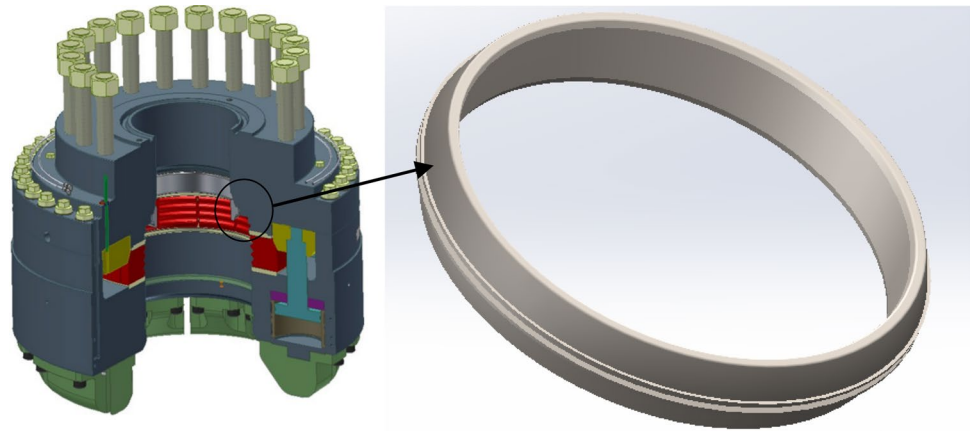
Furthermore, compared with onshore oil and gas production systems, subsea production systems are hundreds of meters to several kilometers under the water, which leads to significant production risks resulting from operational challenges such as extended maintenance intervals. The working environment of the subsea wellhead connector is exceptionally complex. Not only must it withstand high internal pressure, but must also contend with external factors such as blowout preventers, subsea trees, risers, and surface facilities. Moreover, subsea wellhead connector must also exhibit a stable and reliable connection performance, as well as display safe sealing efficiency to achieve successful operation in such an environment, therefore, requiring meticulous scrutiny to ensure operational safety. The subsea wellhead connector and its metal seal ring are shown in Fig. 1. Since the subsea wellhead connector is subjected to high internal pressure and a highly corrosive environment for extended periods, a metal seal ring is commonly used. The upper and lower hubs of the connector squeeze the seal ring to form a

Technical Editor: Celso Kazuyuki Morooka.

✉ Yufang Li
yufangli@xsyu.edu.cn
Honglin Zhao
zhaohl@cup.edu.cn
Deguo Wang
wdg@cup.edu.cn
Yongbiao Xu
13735273529@163.com

¹ College of Mechanical and Transportation Engineering, China University of Petroleum, Beijing 102249, China

Fig. 1 Subsea wellhead connector and metal seal ring



sealing barrier in the form of a metal-to-metal contact seal. The seal of the subsea wellhead connector is self-tightening, with a matching interference between the metal seal ring and the mating hub, causing the radial compression of the metal seal when preloaded. As the internal pressure rises during operation, the contact stress on the sealing surface of the metal seal ring is reduced by the axial internal pressure force, and increased by the radial internal pressure force, while still meeting the sealing requirements [4].

Many factors affect the sealing performance of the subsea wellhead connector, and the mechanical relationship between the structures is complicated. Thus far, no relevant literature exists to theoretically determine the mathematical relationship between the metal seal contact stress of the subsea wellhead connector and its structural parameters. The American Society of Mechanical Engineers (ASME) Boiler and Pressure Vessel Code VIII-2 systematically analyzes the different types of metal gasket design methods, but the metal seal structure studied in this paper is not within the scope of this standard [5]. Sweeney and Schnakenburg [6] discussed the minimum gasket yield strength requirements and pressure integrity of wellhead connector separation by using direct measurement techniques, finite element analysis (FEA), and full scale strain gage testing. Cao [7] designed a new pull-up metal-to-metal seal suitable for use in the subsea wellhead, actuated by pull-up force, and obtained from the drill pipe. Furthermore, the contact load of the seal ring was analyzed using ABAQUS after being subjected to different preloads. Wang et al. [8] studied the optimum design of a mechanical connector for a subsea pipeline based on the sealing performance. Therefore, the finite element model was created using the ANSYS Parametric Design Language (APDL), and the structure was optimized with the zero-order method. Zhao et al. [9] analyzed the metal sealing performance of the subsea X-tree wellhead connectors at a pressure of 34.5 MPa, while also investigating the influence of preload force and internal pressure on contact stress. Wei et al. [10] used the superposition theorem of elasticity to

deduce the formula of the critical mean contact pressure of a mechanical subsea pipeline connector. The finite element analysis result corresponds with this evaluation. Yun et al. [11] studied the sealing contact characteristics of subsea collet connectors based on the theory of Hertz. Tang et al. [12] investigated the sealing principle and the influence of temperature on the sealing performance of marine unbonded flexible pipes based on hydraulic-thermal finite element modeling. Carpenter [13] proposed a new advanced design concept for the wellhead connector, which can meet the demand of high-pressure and high-temperature (HP/HT) environments, and accommodate various levels of external tension and compression loads. Gawande [14], Haruyama et al. [15], Beghini et al. [16] all studied the sealing performance of the metal sealing gasket from the perspective of the leakage rate. Korndorf [17] proposed a calculation method involving a double-cone ring seal. This method considered the additional bolt force caused by the internal pressure load of the double-cone ring with friction while disregarding the stress of the double-cone ring resulting from preload force. Bertsch and Sige [18] determined the relation formula of the bolt preload, contact pressure and internal pressure of the double-cone ring and explored the sealing mechanism of the double-cone ring during both the preloading stage and the working stage. They indicated that the main factors affecting the double-cone ring seal signified a statically indeterminate problem, which was not suitable for engineering application. Zhang et al. [19] used the contact theory to study the metal seal in the lenticular gasket of the subsea manifold connector. The relationship between the maximum contact pressure of the lenticular gasket and the contact width and preload force was analyzed. The mechanical locking effect of the connector was taken as the objective function to optimize the locking mechanism, but the specific pressure of the seals under operating conditions was not considered relevant. Sawa et al. [20] analyzed the influence of different flange thickness, as well as the number of bolts and gasket widths on the sealing performance of box-shape flange connections

with gaskets under internal pressure using the finite element method. Nash et al. [21] used the finite element method to analyze the behavior of metal-to-metal taper–hub flanges and studied the effect of flange thickness, taper–hub thickness, and length on the sealing performance. Krishna [22] considered the nonlinear material properties and permanent deformation of the gasket. A three-dimensional FEA was performed on the flange joints by taking into account the experimentally obtained loading and unloading characteristics of the gaskets, and analyzing the influence of contact stress distribution on the sealing performance. Nelson and Prasad [23] formulated the bolt preload required for the safe operation of twin gasket joints by modifying the ASME code. Furthermore, the design parameters such as individual gasket widths and the spaces between the gaskets are diversified to examine the contact pressure of the twin gasket joints, showing tolerance for higher internal pressure. Murtagian et al. [24] investigated the efficacy of the stationary metal-to-metal seals of the tubular connections using FEA and laboratory tests and developed a sealing criterion that can be used for the comparison, qualification and future performance improvements of different metal-to-metal seals, particularly those used in the petroleum industry.

The majority of studies conducted in the past focused on the calculation of the bolt load, as well as the relationship between the bolt load and both the contact stress and the contact width using the finite element method. However, the theoretical relationship between the contact stress and the structural parameters of the metal seal has not been established. The metal seal of the subsea wellhead connector presents a challenge involving direct contact. Since various factors affect sealing efficiency, the relationship between contact stress and related parameters such as contact width, and deformation amount, is unclear and cannot be obtained directly via the selected test method. Usually, the finite

element method is used to verify the sealing performance of the contact stress, the amount of compression, and the preloading load. Therefore, since determining the finite element model and calculation requires additional time, it is necessary to establish a theoretical paradigm of the mathematical relationship between the metal seal contact stress of the subsea wellhead connector and the relevant structural parameters.

This paper focuses on the analysis of the sealing mechanism of the metal seal ring of the subsea wellhead connector. Therefore, the relationship between the contact stress and the structural parameters of the seal ring is obtained, while the finite element method is used to verify the rationality of the theoretical calculation. Finally, by constructing a test device to evaluate the metal seal of the subsea wellhead connector, the relationship between preload force and contact width, as well as the amount of compression is analyzed. Furthermore, the maximum sealing pressure under different preload forces is studied. This paper provides a theoretical calculation method for designing the metal seal ring of the subsea wellhead connector.

2 Analysis of the sealing mechanism of the subsea wellhead connector

2.1 Mechanical analysis under preloading conditions

2.1.1 Mechanical analysis of the driving pistons

The subsea wellhead connector mainly consisted of an outer body, a driving piston, an action ring, a metal seal ring, and a lock block [25]. Figure 2 shows the force transmission relationship between the components of the wellhead connector

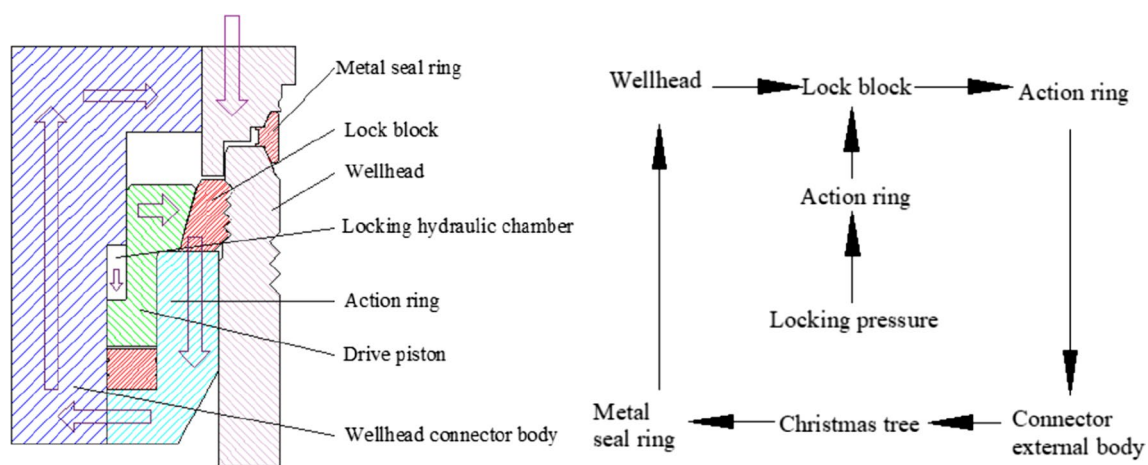


Fig. 2 Mechanical analysis of the wellhead connector in preloading conditions

during the preloading process. The driving piston moved vertically downward under the control pressure, pushing the lock block to move radially, which provided an axial preload for the intermeshing of the lock block and the wellhead. The axial preload force provided by the lock block was transmitted to the entire tree through the connector body, which drove the entire tree downward, compressing the metal seal ring, and sealing the subsea tree and wellhead.

A simplified preloading physical model of the subsea wellhead connector is shown in Fig. 3, in which the driving piston was simplified to triangle 1, and the lock block to triangle 2. The active force prompted driving piston 1 to move in a vertical direction. Lock block 2 made contact with the oblique side of driving piston 1, pushing lock block 2 in a horizontal direction until it was located close to the fixed

surface on the right side, after which the preloading process was complete.

When the preload force was applied to the driving piston, as shown in Fig. 4, it was subjected to the control pressure P , and moved downward relative to the lock block. F_{N1} is the positive pressure of the contact surface between the driving piston and the lock block, and f_{N1} is the friction force. F_s is the combined force of the positive pressure and the friction force, while F_x is the radial elastic force of the driving piston. $D/2$ and $d/2$ are the inner and outer diameters of the driving piston, respectively. Furthermore, α is the contact angle between the driving piston and the lock block, and f_1 is the friction angle between the driving piston and the lock block contact surface.

The locking force F_L generated by the control pressure:

Fig. 3 A simplified model of the preloading conditions

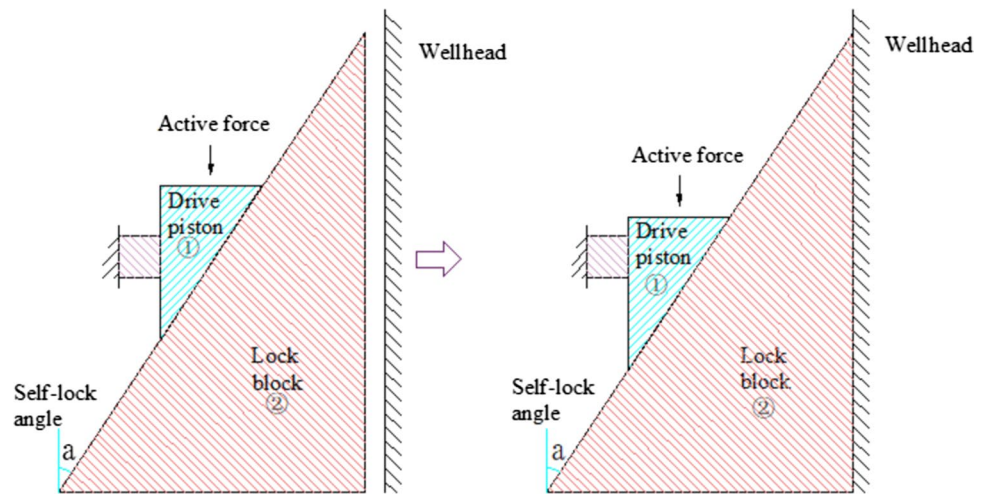
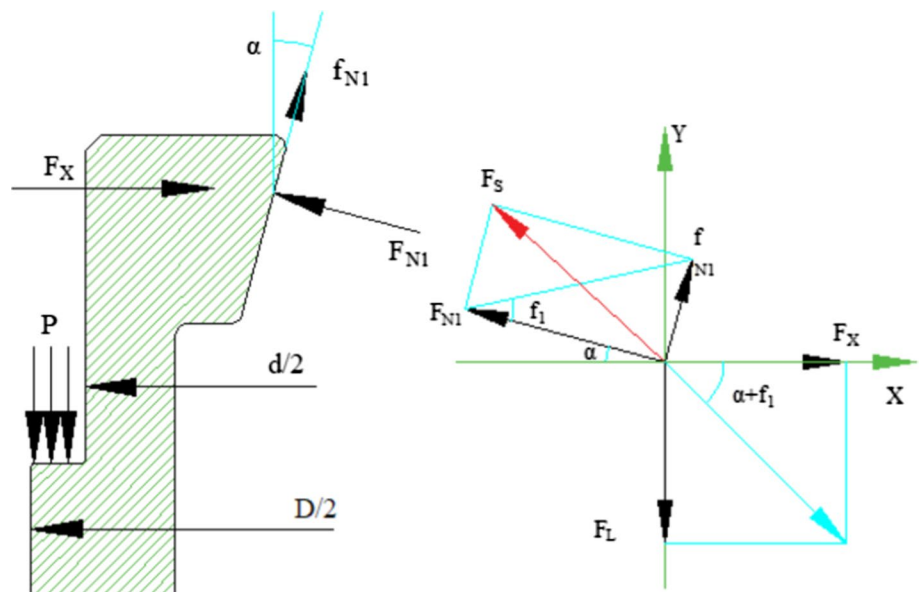


Fig. 4 Mechanical analysis of the driving piston in preloading conditions



$$F_L = p\pi \left(\frac{D^2}{4} - \frac{d^2}{4} \right). \tag{1}$$

Friction force f_{N1} between the driving piston and the contact surface of the lock block:

$$f_{N1} = \frac{F_L}{\sin(\alpha + f_1)} \sin f_1. \tag{2}$$

The driving piston applied positive pressure F_{N1} to the lock block:

$$F_{N1} = \frac{F_L}{\sin(\alpha + f_1)} \cos f_1. \tag{3}$$

2.1.2 Mechanical analysis of the lock block

The force of the lock block in the preloading state is shown in Fig. 5. Under the dynamic action of the driving piston, the radial movement of the lock block gradually engaged with the wellhead cogging. Due to the axial interference of the lock block and the wellhead, the lock block drove the subsea connector and the subsea tree downward where the wellhead was fixed, compressing the metal seal ring and establishing the connection between the subsea tree and the subsea wellhead.

The static balance equations in the X-axis and Y-axis directions were established by examining the lock block:

$$\begin{cases} \frac{F_{N1}}{\cos f_1} \cos(\alpha + f_1) - \frac{F_{N2}}{\cos f_2} \cos(\beta - f_2) - F_N \tan f = 0 \\ F_N - \frac{F_{N1}}{\cos f_1} \sin(\alpha + f_1) - \frac{F_{N2}}{\cos f_2} \sin(\beta - f_2) = 0 \end{cases} \tag{4}$$

where f is the friction angle between the action ring and the contact surface of the lock block, f_2 is the friction angle between the wellhead and the tooth groove contact surface of the lock block, F_N is the support force of the action ring on the lock block, and F_{N2} is the meshing force between the lock block and the wellhead cogging. Additionally, f_N is the friction between the action ring and the lock block, f_{N1} is the friction between the drive piston and the pressed surface of the lock block, f_{N2} is the friction between the lock block and the wellhead cogging, and β is the angle of the mating surface of the lock block.

The axial preload force F_N provided by the lock block in the preloaded state:

$$F_N = F_{N1} \left[\frac{\cos(\alpha + f_1) \sin(\beta - f_2) + \cos(\beta - f_2) \sin(\alpha + f_1)}{\cos f_1 [\cos(\beta - f_2) + \sin(\beta - f_2) \tan f]} \right]. \tag{5}$$

The meshing force between the lock block and the wellhead cogging F_{N2} :

$$F_{N2} = F_{N1} \left[\frac{\cos f_2 [\cos(\alpha + f_1) - \sin(\alpha + f_1) \tan f]}{\cos f_1 [\cos(\beta - f_2) + \sin(\beta - f_2) \tan f]} \right]. \tag{6}$$

2.1.3 Mechanical analysis of the subsea tree

The force analysis of the subsea tree during the preloading process is shown in Fig. 6. When the connector was placed in the appropriate position, the axial preload force provided by the lock block applied preload force to the metal seal ring via the action ring and the body of the subsea tree, which applied axial preload force to the metal seal ring.

Fig. 5 Mechanical analysis of the lock block in preloading conditions

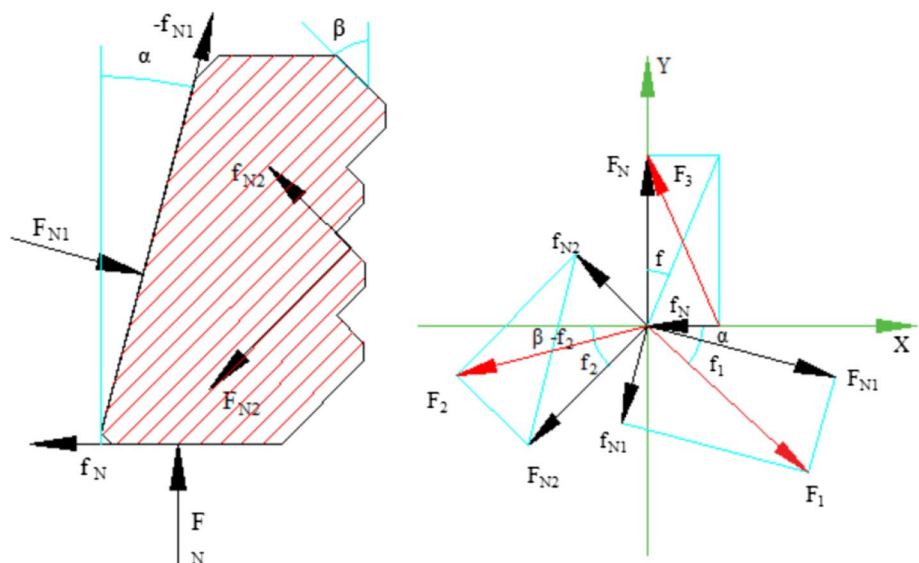
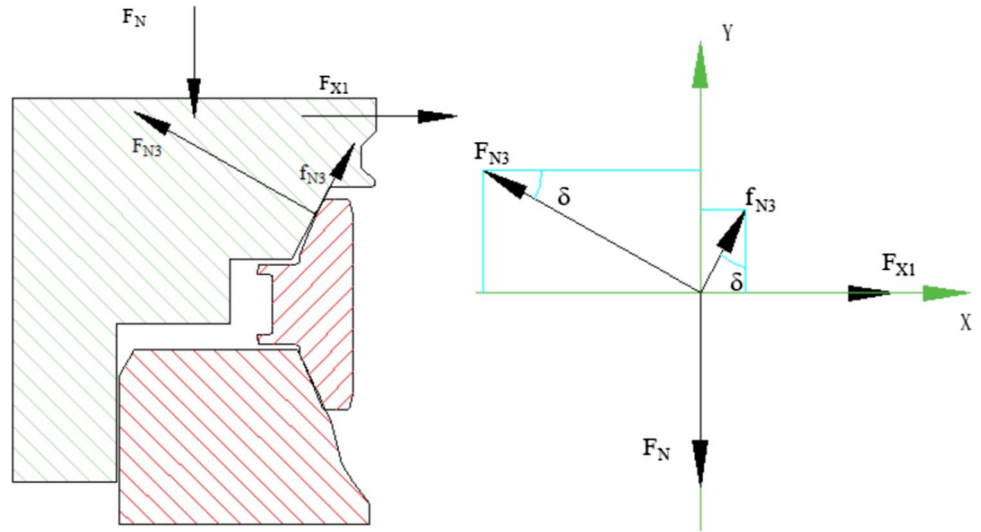


Fig. 6 Mechanical analysis of the subsea tree body in preloading conditions



The movement of the subsea tree exhibited a downward tendency, while the frictional force f_{N3} of the contact surface of the tree and the metal seal ring moved upward. Furthermore, f_3 denotes the friction angle between the metal seal ring and the sealing groove, F_{X1} is the radial elastic reaction force, and F_{N3} is the normal force provided by the subsea tree to the metal seal.

The normal force F_{N3} of the metal seal in the preloaded state:

$$F_{N3} = \frac{F_N}{\sin \delta + \tan f_3 \cos \delta} \tag{7}$$

Friction force f_{N3} between the contact surface of the tree and the metal seal:

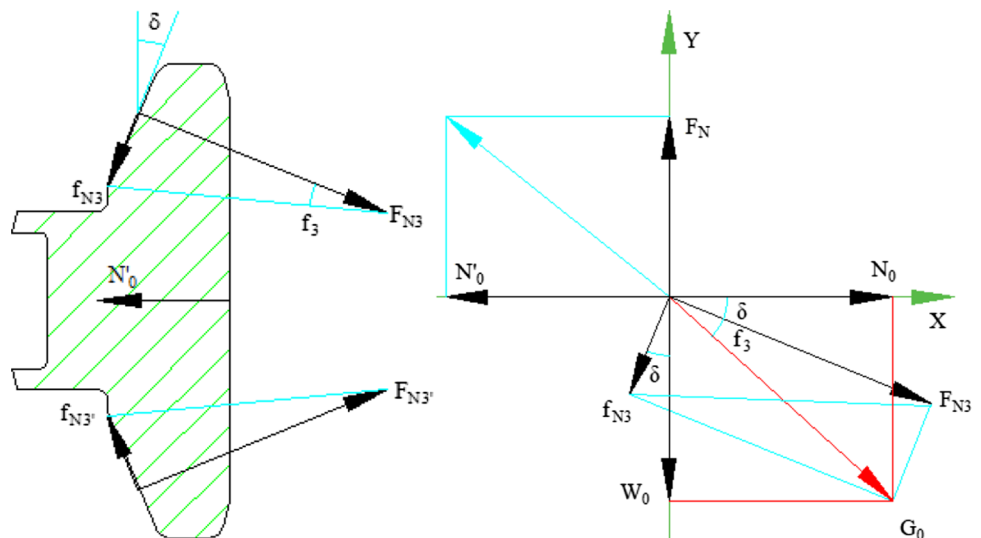
$$f_{N3} = F_{N3} \tan f_3 = \frac{F_N}{\sin \delta + \tan f_3 \cos \delta} \tan f_3. \tag{8}$$

2.1.4 Mechanical analysis of the metal seal ring

As shown in Fig. 7, the metal seal was subjected to the normal force F_{N3} from the subsea tree during preloading. The subsea tree moved downward, while the upper part of the metal seal moved upward. Therefore, the direction of the friction force f_{N3} was downward.

The resultant force G_0 on the sealing surface could be converted into axial and radial components. The metal seal ring was axially compressed by axial component force W_0 , while the radial component force N_0 was responsible for radial compression. The axial preload force W_0 and radial preload force N_0 were:

Fig. 7 Mechanical analysis of the metal seal ring of the well-head connector in preloading



$$W_0 = \frac{F_{N3}}{\cos f_3} \sin(\delta + f_3) \tag{9}$$

$$N_0 = \frac{F_{N3}}{\cos f_3} \cos(\delta + f_3). \tag{10}$$

The metal seal ring was compressed during preloading, and when the radial deformation was 2Δ , the circumferential strain ϵ_θ and the corresponding circumferential stress σ_θ were:

$$\epsilon_\theta = \frac{\pi(D_1 - 2\Delta) - \pi D_1}{\pi D_1} = -\frac{2\Delta}{D_1} \tag{11}$$

$$\sigma_\theta = E_R \epsilon_\theta = -E_R \frac{2\Delta}{D_1} \tag{12}$$

Among them, D_1 is the median diameter of the metal seal ring, while E_R signifies the elastic modulus.

Due to its axisymmetric structure, half a seal ring was acquired for static balance analysis, and the force is shown in Fig. 8. The resilience of the seal ring in the circumferential length was $N_0/\pi D_1$, which could be obtained with static balance:

$$\int_0^\pi \frac{N_0}{\pi D_1} R_1 d\varphi \sin \varphi = -2F_R \sigma_\theta = 2F_R E_R \frac{2\Delta}{D_1} \tag{13}$$

where F_R is the cross-sectional area of the seal ring, R_1 is 1/2 of the median diameter D_1 , and φ is the angle between the resilience force in the unit circumferential length and the cross section of the semi-seal ring.

From Eq. (13):

$$N_0 = \frac{4\pi F_R E_R \Delta}{D_1}. \tag{14}$$

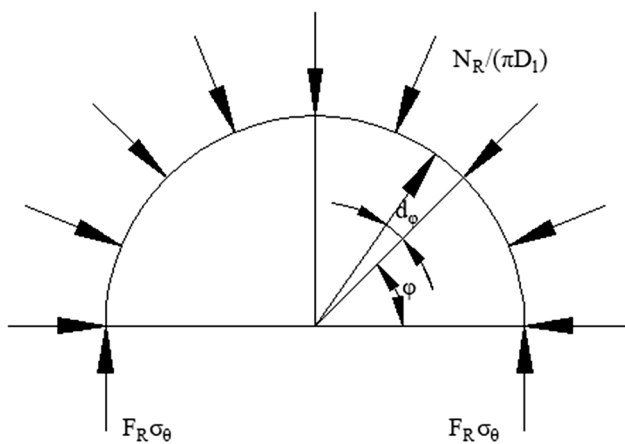


Fig. 8 Static balance of metal seal ring

The initial sealing conditions for metal seal ring of the subsea wellhead connector dictated that the contact stress should not be less than the initial seal specific pressure. According to the geometric characteristics of the contact surface, the metal seal ring studied in this paper could refer to the ring gasket, when the gasket material was stainless steel. The initial seal specific pressure was 180 MPa.

From Eqs. (9) and (10), the relationship between the preload seal contact stress and the amount of radial deformation was obtained:

$$q_0 = \frac{4F_R E_R \Delta}{D_1^2 b} \cdot \frac{\cos f_3}{\cos(\delta + f_3)} = \frac{W_0}{\pi D_1 b} \cdot \frac{\cos f_3}{\sin(\delta + f_3)}. \tag{15}$$

2.2 Mechanical analysis under operating conditions

2.2.1 Force analysis under operating conditions

Due to the pressure in the production channel during the subsea oil and gas manufacturing process, the subsea tree tended to rise, as shown in Fig. 9. The axial force of the connector was composed of four parts: the axial load W_0 during preloading, the axial load W_p caused by the internal pressure acting on the connector, the axial load W_1' caused by internal pressure acting on the inner side of the seal, and the axial load W_2' resulting from the resilience of the metal seal when it was preloaded.

1. The axial load W_p caused by the internal pressure acting on the connector

$$W_p = -ps_p \tag{16}$$

where s_p is the area under axial internal pressure, and p is the internal working pressure, MPa.

2. The axial load W_1' caused by internal pressure acting on the inner side of the seal.

The internal pressure acted on the inner side of the seal ring enabling it to generate a radial self-tightening force. This force exerted a corresponding axial force W_1 , as well as a corresponding normal pressing force F_{N1} on the sealing surface. The radial self-tightening force of the single sealing surface of the metal seal ring was $N_p/2$.

$$N_p = \pi D_1 h p \tag{17}$$

where h is the height at the inner diameter of the metal seal.

The connector tended to rise in conjunction with higher internal pressure, while the metal seal ring exhibited a downward tendency. The frictional force of the sealing surface F_{f1} , the combined force of the frictional force F_{f1} , and the normal force F_{N1} obtained the radial self-tightening force

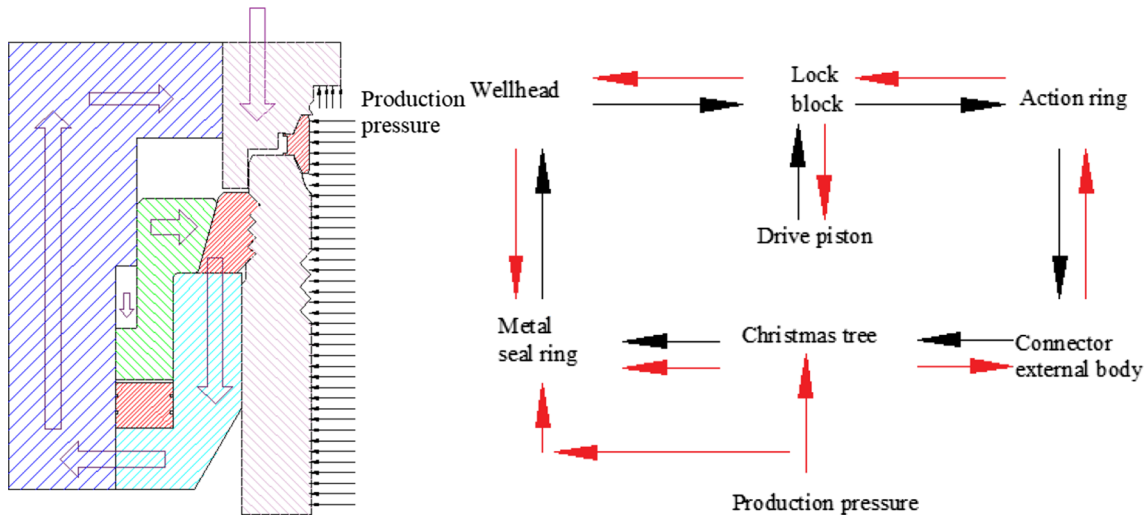


Fig. 9 Mechanical analysis of the wellhead connector in operating conditions

$N_p/2$, as well as the axial force W_1 . The force analysis of the sealing surface is shown in Fig. 10.

$$W_1 = \frac{N_p}{2} \cdot \tan(\delta - f_3) \tag{18}$$

W_1' and axial force W_1 were mutually reactive:

$$W_1' = -W_1 \tag{19}$$

- The axial load W_2' resulted from the resilience of the metal seal when it was preloaded.

Due to the action of the internal pressure, the connector was raised, and the amount of radial compression that accrued when the seal ring was preloaded was released, which caused a change in the preloading elastic force. The resilience force acting on the sealing surface was $N_0'/2$.

$$N_0' = \frac{4\pi F_R E_R \Delta'}{D_1} \tag{20}$$

where Δ' is the amount of radial compression after the rebound.

The normal force and the friction force on the contact surface of the seal ring were combined and converted into a radial force $N_0'/2$ and an axial force W_2 :

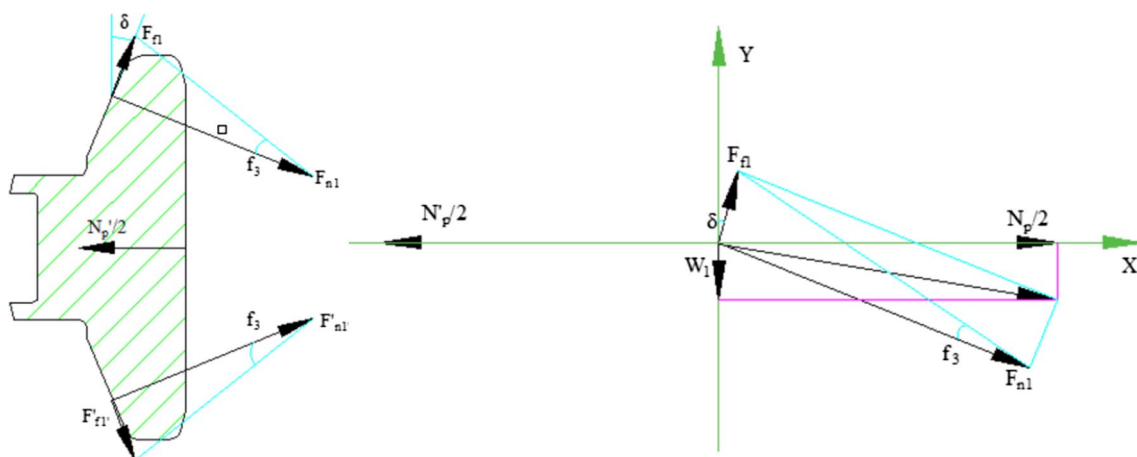


Fig. 10 Force analysis of the internal pressure of the sealing surface under operating conditions

$$W_2 = \frac{N'_0}{2} \cdot \tan(\delta - f_3) = \frac{2\pi F_R E_R \Delta'}{D_1} \tan(\delta - f_3). \tag{21}$$

W_2' and axial force W_2 were mutually reactive:

$$W_2' = -W_2 = -\frac{2\pi F_R E_R \Delta'}{D_1} \tan(\delta - f_3). \tag{22}$$

From this, the connector back force could be expressed as:

$$W_\Sigma = W_p + W_1' + W_2' = -ps_p - \frac{1}{2}\pi D_1 h p \tan(\alpha - \rho) - \frac{2\pi F_R E_R \Delta'}{D_1} \tan(\alpha - \rho). \tag{23}$$

$$W'' = \frac{\left[\frac{1}{2}\pi D_1 h \tan(\delta - f_3) - \frac{2\pi F_R E_R L_1 s_p}{D_1 E_1 s_1} \tan(\delta - f_3) \tan \delta \right] p + \frac{2\pi F_R E_R}{D_1} \left(\Delta + \frac{W_0 L_1}{E_1 s_1} \tan \delta \right) \tan(\delta - f_3)}{1 + \frac{2\pi F_R E_R L_1}{D_1 E_1 s_1} \tan(\delta - f_3) \tan \delta}. \tag{28}$$

2.2.2 Mechanical analysis of the operating process

The internal pressure was gradually increased, while the axial force it generated canceled the axial preload, with a pressure value of:

$$p_{\min} = \frac{W_0}{\frac{1}{2}\pi D_1 h \tan(\sigma - f_3) + s_p}. \tag{24}$$

The radial load $N_p/2$, and the amount of pre-compression rebound force $N_R/2$, generated contact stress on the sealing surface, while the pre-tightening force of the sealing surface was the lowest.

As the pressure continued to rise, the connector was raised, and only W'' supplied contact pressure on the surface of the seal:

$$W'' = \frac{N_p + N'_0}{2} \cdot \tan(\delta - f_3) = F_n \frac{\sin(\delta - f_3)}{\cos f}. \tag{25}$$

The contact stress q was:

$$q = \frac{N'_0 + N_p}{2\pi D_1 b} \cdot \frac{\cos f_3}{\cos(\delta - f_3)} = \frac{W''}{\pi D_1 b \tan(\delta - f_3)} \cdot \frac{\cos f_3}{\cos(\delta - f_3)}. \tag{26}$$

2.2.3 Contact stress analysis of the metal seal during the operational process

The radial compression amount Δ' was related to the internal pressure p , and represented an unknown amount in Eq. (26). Therefore, Eq. (26) could not fully express the relationship between the operational contact stress q and the internal pressure p .

ΔL represented the deformation of the connector resulting from the axial action of the internal pressure, and the geometric relationship between ΔL and Δ' was obtained:

$$\Delta - \Delta' = \Delta L \tan \delta = (ps_p + W'' - W_0) \frac{L_1}{E_1 s_1} \tan \delta \tag{27}$$

where E_1 is the elastic modulus of the connector, L_1 is the length of the elongate connector member, and S_1 is the cross-sectional area of the connector elongate member.

From Eqs. (26) and (27), it could be derived:

Under the operating conditions, the operating contact stress q of the metal seal of the subsea wellhead connector was:

$$q = \frac{\left[\frac{1}{2}\pi D_1 h - \frac{2\pi F_R E_R L_1 s_p}{D_1 E_1 s_1} \tan \delta \right] p + \frac{2\pi F_R E_R}{D_1} \left(\Delta + \frac{W_0 L_1}{E_1 s_1} \tan \delta \right)}{1 + \frac{2\pi F_R E_R L_1}{D_1 E_1 s_1} \tan(\delta - f_3) \tan \delta} \cdot \frac{\cos f_3}{\pi D_1 b \cos(\delta - f_3)}. \tag{29}$$

2.3 Strength design for the metal seal ring structure

Better sealing efficiency was achieved when the contact stress on the contact surface was higher. However, when the contact pressure increased to a specific level, the metal seal ring entered a plastic state, causing the failure of the metal seal ring structure. Therefore, the upper limit of the contact pressure had to be controlled to evaluate the strength of the seal ring.

2.3.1 Preload conditions

In preloading conditions, the dangerous section of the metal seal ring was the sealing surface, which was set as the reference surface. The principal stresses were denoted by normal stress σ_0 on the sealing surface, shear stress τ_0 , and hoop stress σ_θ , respectively. Their values were:

$$\sigma_0 = -\frac{W_0 \cos f_3}{\pi D_1 b \sin(\delta + f_3)} \tag{30}$$

$$\tau'_0 = \frac{W'' \sin f_3}{\pi D_1 b \sin(\delta - f_3)} \tag{34}$$

$$\tau_0 = -\frac{W_0 \sin f_3}{\pi D_1 b \sin(\delta + f_3)} \tag{31}$$

$$\sigma'_\theta = -\frac{2\Delta'}{D_1} E_R. \tag{35}$$

$$\sigma_\theta = -\frac{2\Delta}{D_1} E_R. \tag{32}$$

σ_s is the yield strength of the seal material. The stress evaluation was performed using the fourth strength theory, which is a distortion energy density theory suitable for conditions where similar three-way stress can cause plastic deformation. The criterion is:

2.3.2 Operating conditions

In operating conditions, the dangerous section of the metal seal ring was also the sealing surface, which was set as the reference surface. The principal stresses were represented by normal stress σ'_0 on the sealing surface, shear stress τ'_0 , and hoop stress σ'_θ , respectively. Their values were:

$$\sigma'_0 = -\frac{W'' \cos f_3}{\pi D_1 b_1 \sin(\delta - f_3)} \tag{33}$$

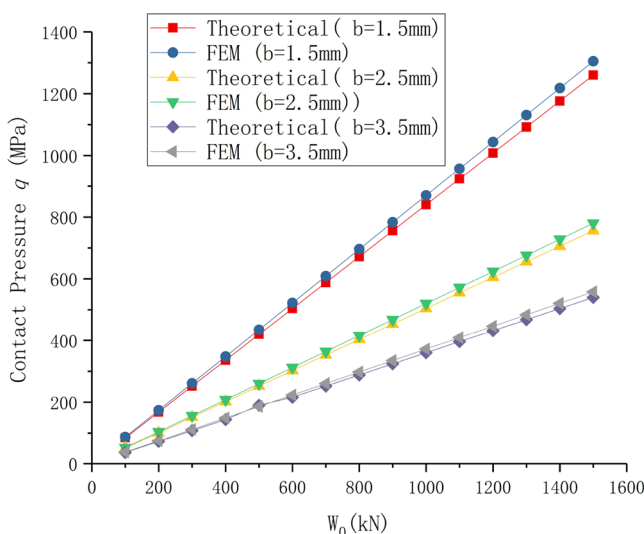
$$\sqrt{\frac{1}{2}[(\sigma_1 - \sigma_2)^2 + (\sigma_1 - \sigma_3)^2 + (\sigma_2 - \sigma_3)^2]} \leq [\sigma_s]. \tag{36}$$

3 FEA of the metal seal ring of the subsea wellhead connector

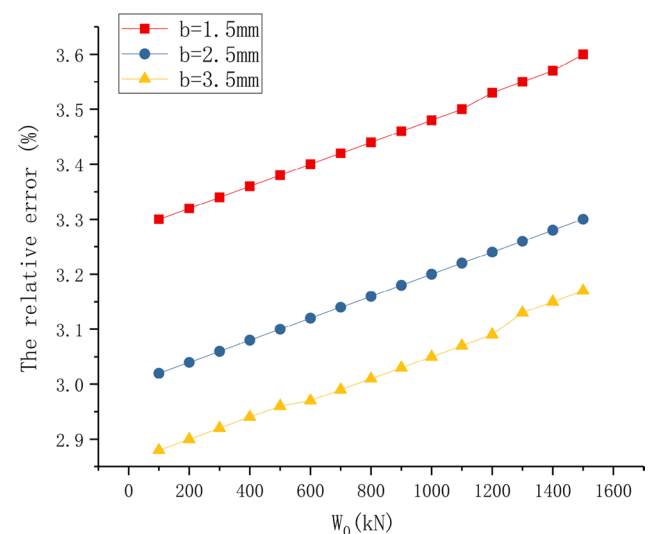
The 18-3/4 in. subsea wellhead connector metal seal of an oilfield in the South China Sea was used as an example, with a design pressure of 69 MPa. The numerical model was established using the finite element method to verify the accuracy of the theoretical calculation. The axisymmetric model of the subsea wellhead connector was established with ANSYS 16.0 software. The displacement load was applied to the upper and lower contact faces of the metal seal ring, causing pressure from above and below, respectively. Therefore, the internal pressure was applied during operating conditions. The calculation results of the contact stress and contact width on the sealing surface of the metal

Table 1 Main parameters of numerical model

Parameter	Value	Parameter	Value
D_1	523.82 mm	L_1	210 mm
h	101.6 mm	s_p	182,177.6407 mm ²
F_R	2892.96 mm ²	E_1	2.09 × 10 ⁵ MPa
E_R	1.95 × 10 ⁵ MPa	s_1	584,668 mm ²



(a) Axial preload vs. contact pressure



(b) The relative error

Fig. 11 Axial preload versus contact pressure

seal ring were analyzed. The main calculation parameters are shown in Table 1.

According to formulas (15), (29), (36), combined with the structural parameters in Table 1, the axial preloading compression Δ was 0.101–0.201 mm, and the corresponding axial preload force W_0 was 892.5–1802.9 kN.

3.1 The effect of axial preload on contact stress

As shown in Fig. 11, when the different contact widths b were 1.5 mm, 2.5 mm, and 3.5 mm, respectively, the relationship between the contact stress and the axial preload force was calculated via the theoretical method and the finite element method established in this paper. When the contact width remained constant, the contact stress of the metal seal ring increased in conjunction with a rise in the preload force, and was proportional to the relationship. When the axial preload force remained constant, the contact stress decreased rapidly as the contact width increased, which was not conducive to sealing efficacy. The maximum relative error between the FEA and the theoretical calculation was 3.6%. When the axial preload force was within the given range of 892.5–1902.9 kN, the preload contact stress exceeded the preload seal specific pressure (180 MPa), allowing the metal seal ring to meet the sealing requirements and ensuring sealing efficiency.

3.2 The effect of contact width on contact stress

Based on the theoretical method and finite element method established in this paper, the relationship between contact

stress and contact width under different axial preload forces was calculated. As shown in Fig. 12 the contact stress decreased in conjunction with increased contact width, while contact stress was inversely proportional to the contact width. At the same contact width, a more substantial axial preload induced a more significant corresponding contact stress, and the maximum relative error of the two calculation methods was 4.9%. When the contact width ranged between 1 and 6 mm, the preload contact stress exceeded the preload seal specific pressure (180 MPa), allowing the metal seal ring to meet the sealing requirements and ensuring sealing efficiency.

The preload contact stress and operational contact stress could be expressed as follows:

Preload contact stress:

$$q_0 = \frac{W_0}{\pi D_m b} \cdot \frac{\cos f_3}{\sin(\delta + f_3)} \tag{37}$$

Operational contact stress:

$$q = \frac{\frac{4F_R E_R \Delta'}{D_1} + D_1 h p}{2D_1 b} \cdot \frac{\cos f_3}{\cos(\delta - f_3)}. \tag{38}$$

It was evident from the two equations above that the width b of the sealing surface increased, while the other parameters remained constant, and the preload contact stress, as well as the operating contact stress declined rapidly, which was not conducive to sealing efficacy. For preload contact stress, increasing the contact width multiplied the required axial preload force, which made locking

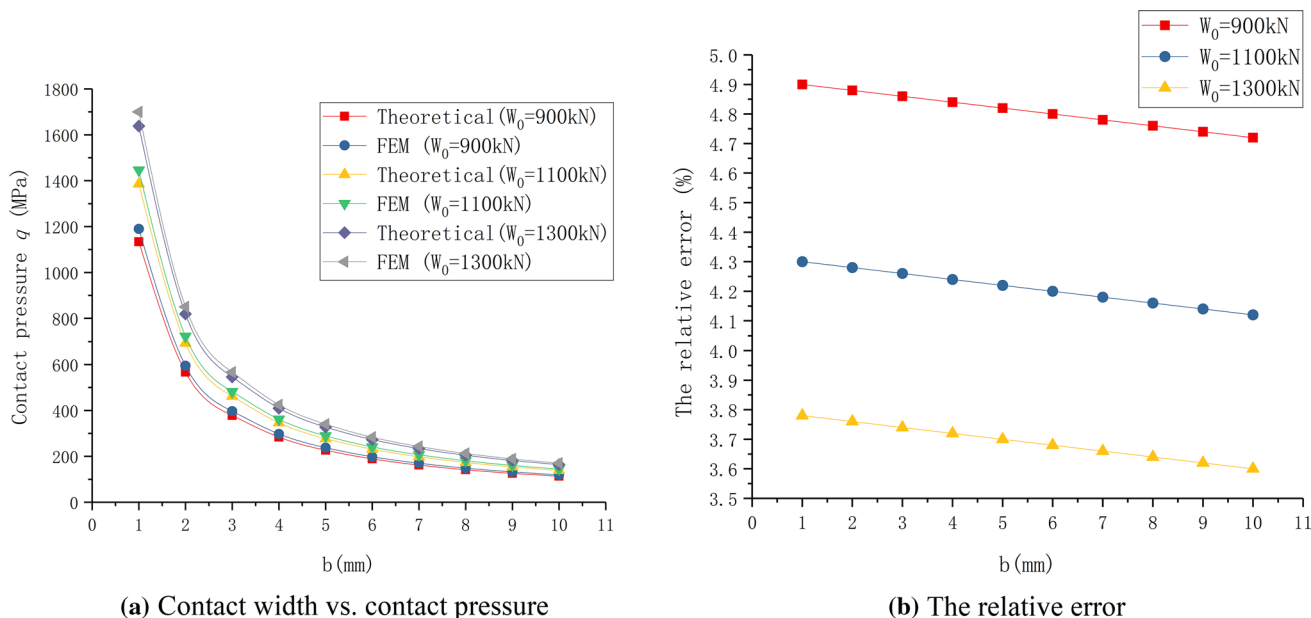


Fig. 12 Contact width versus contact pressure

the connector-mounting tool difficult. For the operational contact stress, increasing the width necessitated an increase in the cross-sectional dimension of the metal seal ring, especially its height. Therefore, the overall structure of the connector became too large, which contradicted the design principle of a convenient structure. However, if the contact width was too small, it reduced the adaptability of the seal to the manufacturing defects and roughness. When the metal seal ring was installed, the relative movement of the sealing pair might easily cause the sealing surface to be damaged or scratched. The contact width of the sealing surface significantly influenced contact stress. Therefore, given the design rationality and the sealing reliability, it was generally preferred to use a narrow sealing surface when the width was sufficient.

3.3 The effect of preload compression on contact stress

As shown in Fig. 13, the different contact widths b were denoted by 1.5 mm, 2.5 mm, 3.5 mm, respectively. When the contact width remained constant, the contact stress of the metal seal increased in conjunction with the radial compression and was proportional. When the amount of compression remained constant, the operating contact stress exhibited a rapid decline with an increase in the contact width, which was not conducive to sealing efficiency. The FEA results were consistent with the theoretical calculation results, while the maximum relative error was 4%.

It was apparent from Eq. (15) that the amount of radial pre-compression Δ significantly influenced the preload contact stress of the metal seal ring. When the structure remained constant, a higher amount of radial

pre-compression Δ was evident with a rise in pre-tightening contact stress. When preloading, it was easier to maintain the compression rebound during its operation when the radial pre-compression of the seal ring was more extensive and could continuously provide it with rebound contact stress. The adaptability of the metal seal ring to pressure fluctuations was significantly improved by appropriately increasing its distance from the supporting surface. Therefore, the amount of radial pre-compression could be more substantial in the design, which was convenient for enhancing the metal seal ring to adapt to pressure fluctuations, ensuring adequate sealing performance. However, if the amount of radial pre-compression Δ was not large enough, it could easily cause the seal ring to collapse or the seal ring sealing surface to be damaged, resulting in seal failure. From this analysis it was evident that the preferable amount of radial pre-compression Δ was 0.1–0.2 mm.

3.4 The effect of working pressure on contact stress

The relationship between working pressure and operating contact stress is shown in Fig. 14a, b. The value $\Delta = 0.1$ mm corresponded with $W_0 = 892.5$ kN, while $\Delta = 0.2$ mm corresponded with $W_0 = 1785$ kN and was calculated using Eq. (15). From this, it is clear that the preload contact stress satisfies the initial sealing conditions.

As shown in Fig. 14a, the theoretical calculation of the preload contact stress and the finite element calculation values were 562.3 MPa and 580 MPa, respectively, which exceeded the initial seal specific pressure of 180 MPa. Moreover, the operational contact stress of the metal seal ring rose with an increase in working pressure. The contact stress initially decreased followed by an increase. When the

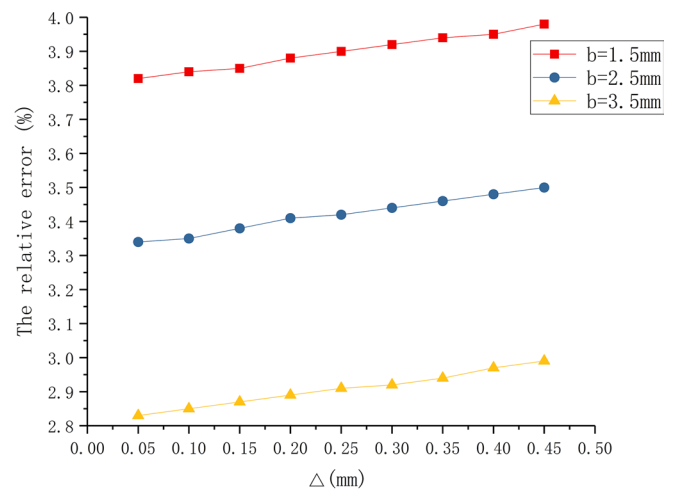
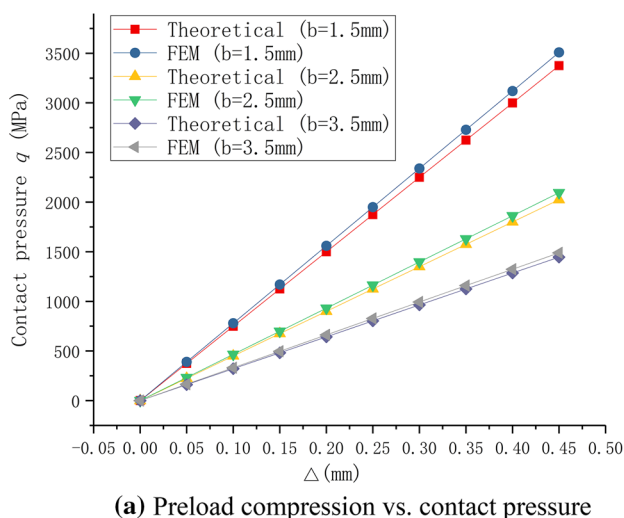


Fig. 13 Preload compression versus contact pressure

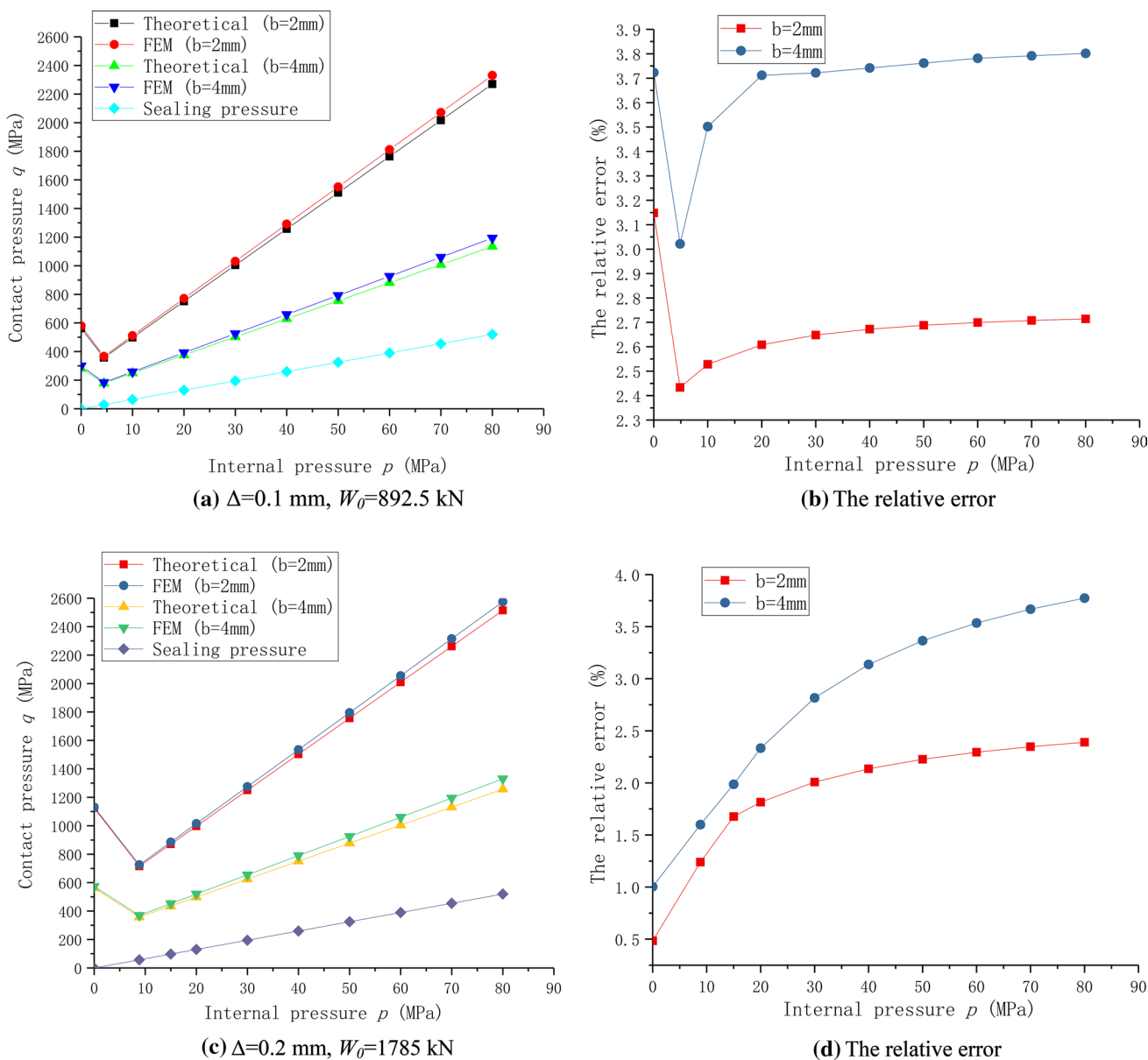


Fig. 14 Internal pressure versus contact pressure

working pressure was about 4.43 MPa, the operating contact stress exhibited a minimum value. The theoretical calculation and the finite element calculation were 357.5 MPa and 366.2 MPa, respectively, which exceeded the operating seal specific pressure $y = mp = 28.79$ MPa. Moreover, the operating contact stress engaged with the working pressure and increased linearly, while the theoretical calculation was consistent with the finite element calculation trend, and the maximum relative error was 3.8%. The operating contact stress curve showed that a more extensive contact width induced lower operating contact stress, which was not conducive to sealing efficacy. Therefore, it was necessary to

increase the axial preload or select a smaller contact width to achieve a higher operating contact stress.

A comparison between Fig. 14a, c, indicated that a higher amount of radial pre-compression Δ increased the corresponding operating contact stress, which was beneficial to sealing efficiency. If the contact width remained the same and $b=2$ mm, the slope of the curve by theoretical calculation and finite element fitting was about 25.3, as shown in Fig. 14a. Figure 14c shows that when $b=2$ mm, the slope of the curve by theoretical calculation and finite element fitting was about 25.6, which was similar to when $b=4$ mm. Therefore, it is evident that the contact width affected the slope of the operating contact stress curve. Additionally, the

amount of pre-compression or axial preload force affected the intercept of the contact stress curve.

Further analysis of the metal seal ring, by formula (29):

$$M = \frac{\left[\frac{1}{2} \pi D_1 h - \frac{2 \pi F_R E_R L_1 s_p}{D_1 E_1 s_1} \tan \delta \right]}{1 + \frac{2 \pi F_R E_R L_1}{D_1 E_1 s_1} \tan(\delta - f_3) \tan \delta} \cdot \frac{\cos f_3}{\pi D_1 b \cos(\delta - f_3)} \quad (39)$$

$$N = \frac{\frac{2 \pi F_R E_R}{D_1} \left(\Delta + \frac{W_0 L_1}{E_1 s_1} \tan \delta \right)}{1 + \frac{2 \pi F_R E_R L_1}{D_1 E_1 s_1} \tan(\delta - f_3) \tan \delta} \cdot \frac{\cos f_3}{\pi D_1 b \cos(\delta - f_3)} \quad (40)$$

Consequently, the contact stress of the metal seal in an operational state could be expressed as:

$$q = Mp + N. \quad (41)$$

It was apparent from Eq. (41) that the operating contact stress of the metal seal ring occurred linearly to the internal pressure. As the internal pressure increased, the operating contact stress first decreased followed by a linear increase. When the axial force generated by the pressure canceled the axial preload force, that is, when $p_{\min} = \frac{W_0}{\frac{1}{2} \pi D_1 h \tan(\alpha - \rho) + s_p}$, the operating contact stress reached a minimum value. The internal pressure continued to increase, and the operating contact stress exceeded the operating seal specific pressure to achieve a self-tightening seal.

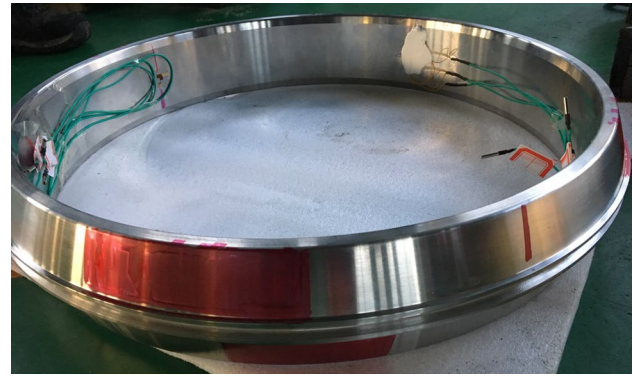


Fig. 16 Metal seal ring for the subsea wellhead connector

4 Experimental research into the metal seal ring of the subsea wellhead connector

To verify the sealing performance of the metal seal of the subsea wellhead connector, a test device was built to evaluate its performance, as shown in Fig. 15. It mainly consists of preload bolts, top and bottom flanges, top and bottom hubs, a metal seal ring, pressure transmitters, a sealing joint, support legs, preload nuts, an oil inlet, and an oil plug.

As shown in Fig. 16, the metal seal ring of the subsea wellhead connector was attached with 120-3AA resistance strain gauges in the axial and radial directions of the inner wall, and the data were recorded by the JC-40 strain measuring instrument. Following installation of the metal seal, a high-torque hydraulic wrench was used to tighten all relevant components. A predetermined preload force was applied to the metal seal ring, while an internal pressure was applied to the device using a hydraulic pump. The pressure

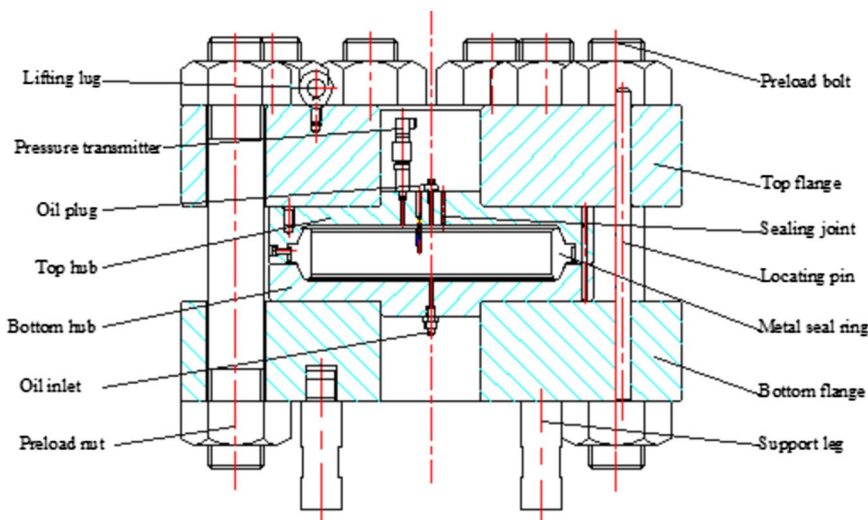
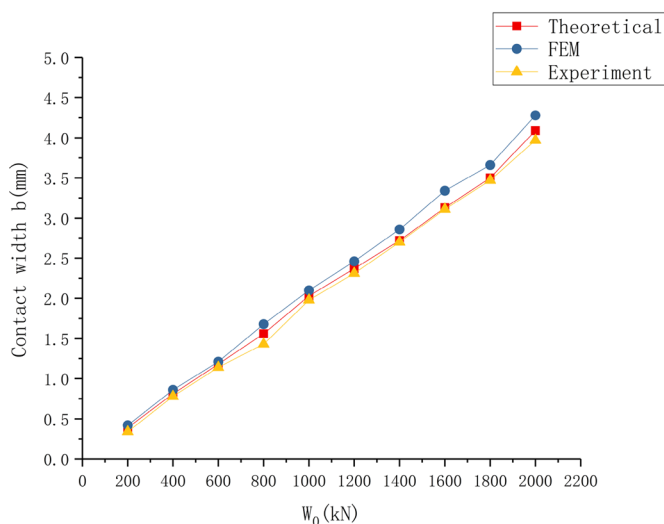
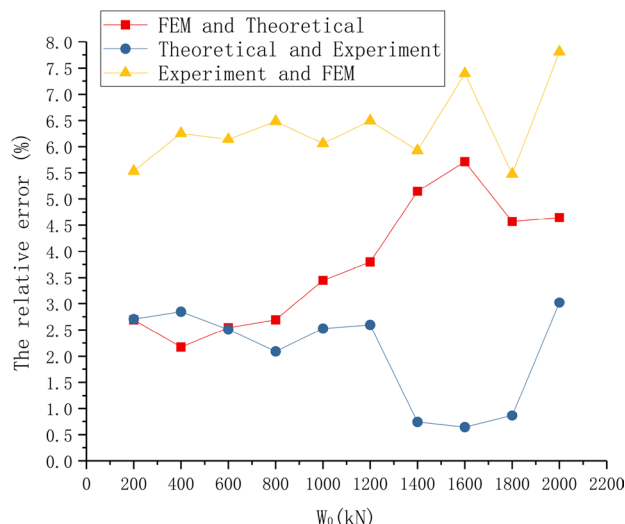


Fig. 15 Sealing test device for the subsea wellhead connector





(a) The contact width vs. preload force



(b) The relative error

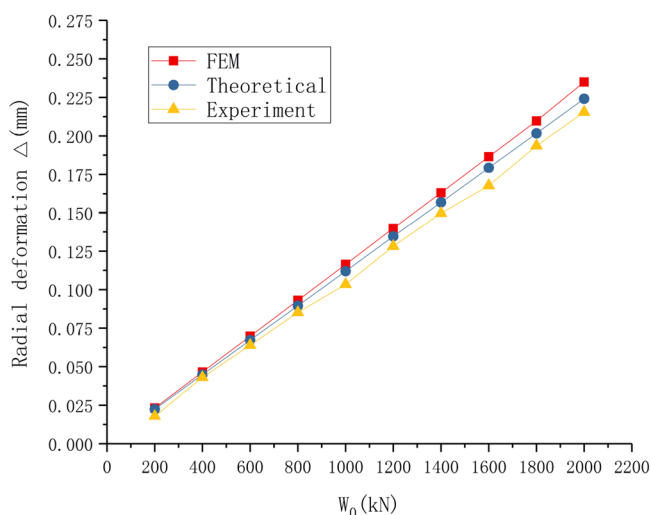
Fig. 17 The relationship between the contact width and preload force

was maintained for 30 min, after which the pressure change in the metal seal ring cavity was measured via the pressure transmitter.

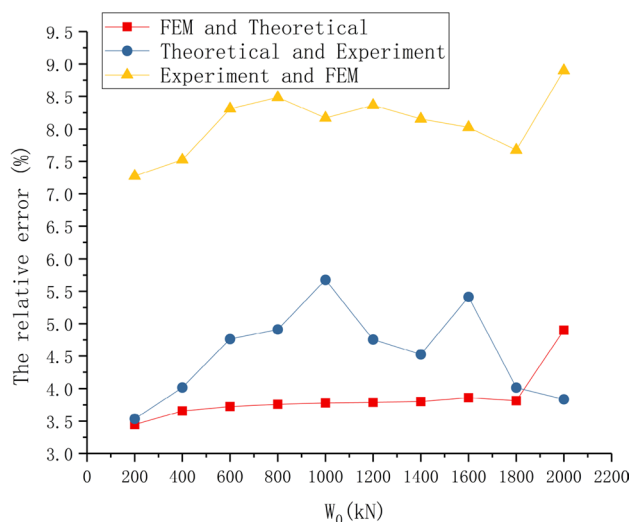
4.1 Contact width and preload force relationship

Under preloading conditions, preloading bolts were used to apply preload force to the hubs and was then unloaded to measure the contact width of the metal seal ring surface. The results of the test, theoretical calculation, and FEA are shown in Fig. 17. The contact width increased in conjunction

with a rise in the preload force and a relative linear change, the test contact width was smaller than both the theoretical calculation and the finite element calculation. When the preload force was 200 kN, the contact width measured with the test was only 0.34 mm. With an increase in the preload force, the contact width measured by the test differed from the theoretical calculation and the finite element calculation. When the preload force was 2000 kN, the theoretically calculated contact width was 4.09 mm, the measured contact width was 3.97 mm, and the maximum relative error was 3.0%, while the contact width calculated with the finite



(a) The compression vs. preload force



(b) The relative error

Fig. 18 The relationship between compression and preload force

Table 2 Test results of preload and maximum sealing pressure

Preload force (kN)	Internal pressure (MPa)	Maximum sealing pressure (MPa)
420	15.0	14.5
540	24.0	23.0
630	30.0	27.8
760	36.0	32.6
850	45.5	42.3
960	52.0	48.2
1120	58.5	55.9
1270	66.0	63.7
1425	74.5	70.2

element was 4.28 mm, the maximum relative error was 7.8%. The relative error range is 0.6–7.8%.

4.2 Compression and preload force relationship

Under preloading conditions, the preload bolts were used to apply preload force to the hubs, which was then unloaded. By measuring the axial displacement between the two hubs, the amount of radial deformation was obtained from the geometric relationship $\Delta = \varepsilon_0 \tan \delta$, while different preload loads were applied and the corresponding axial displacement was measured. The metal seal installation in the test was not entirely flat. Therefore, the average value of multiple points was measured, and the relationship between radial deformation and preload was obtained as shown in Fig. 18.

The radial deformation increased in conjunction with a higher preload force. The test result was slightly lower than the theoretical calculation result, while the finite element calculation result was marginally higher than the theoretical calculation result. Moreover, a lower preload force caused a smaller deformation of the metal seal. The theoretically calculated radial deformation was only 0.0224 mm with a preload force of 200 kN. When the preload force was 2000 kN, the maximum relative error of the radial compression theoretical calculation and test results was 5.7%, while the test results and finite element calculation was 8.9%. The relative error range is 3.4–8.9%.

4.3 Maximum sealing pressure test

To test the relationship between the preload force and the maximum sealing pressure, the preload load was applied to the hubs by the preload bolts. The hydraulic pump applied internal pressure to the sealing test device until the pressure transmitter no longer exhibited an increase. The pressure was maintained for 30 min, and the pressure value was recorded. The obtained pressure value represented the maximum sealing pressure under this preload. The increase

in the preloading load was continued and the steps above were repeated until the internal pressure reached the design pressure. The test results are shown in Table 2. When the preloading load was 1425 kN, the maximum sealing pressure was 70.2 MPa, which increased in conjunction with a rise in the preloading load, indicating that an appropriate increase in the preload force could improve the sealing performance of the subsea wellhead connector.

5 Conclusion

1. The force transmission relationship between the sealing structures of the subsea wellhead connector is established, and the theoretical calculation expression of the contact stress of the metal seal ring under preloading conditions and operating conditions is determined. The main influencing factors of sealing efficiency are preload force, contact width, preload compression, and working pressure. At the same contact width, a higher axial preload force induces a higher corresponding contact stress. When the axial preload force remains constant, the contact stress decreases rapidly in conjunction with the increase in the contact width. Moreover, when the structure remains constant, the preloading contact stress rises with an increase in the amount of pre-compression Δ . As the working pressure increases, the operating contact stress of the metal seal ring first exhibits a decline followed by an increase, and the finite element calculation result is consistent with the theoretical calculation result.
2. The contact stress of the metal seal displays an inflection point during the internal pressure rise, and the contact stress rises in conjunction with an initial increase in the internal pressure of the operating conditions. When the axial force generated by the pressure offsets the axial preload force, that is $p_{\min} = \frac{W_0}{\frac{1}{2}\pi D_1 h \tan(\alpha - \rho) + s_p}$, the contact stress on the surface of the seal reaches a minimum value, while the finite element calculation results also confirm this. When designing the metal seal ring, this minimum contact stress should be carefully considered. Moreover, the sealing surface contact stress satisfies the sealing conditions.
3. A performance test device was constructed to evaluate the metal seal ring of the subsea wellhead connector and verify sealing performance. The test results show an increase in the contact width in conjunction with a rise in preload force, which is approximately linear. Therefore, the test contact width is smaller than both the theoretical calculation and the finite element calculation. The radial deformation increases in conjunction with higher preload force, and the test result is slightly lower than

the theoretical calculation result. The maximum sealing pressure corresponding to different preload forces is verified by using the holding pressure test. The maximum sealing pressure increases together with higher preloading load. When the preloading load is 1425 kN, the maximum sealing pressure is 70.2 MPa. The experimental results show that the designed metal seal ring can adequately meet the sealing requirements.

Acknowledgements This work was financially supported by Ministry of Science and Technology of the People's Republic of China (2016YFC0303701), Ministry of Industry and Information Technology of the People's Republic of China ((2018) 472), National Natural Science Foundation of China (51875578).

Compliance with ethical standards

Conflict of interest The authors declare that they have no conflict of interest.

References

- Bai Y, Bai Q (2012) Subsea engineering handbook. Gulf Professional Publishing, Burlington, pp 6–7
- Bybee K (2007) Dalia subsea production system. In: Society of petroleum engineers, vol 807, pp 62–64
- Perales SA, Kaculi JT (2017) Verification analysis and validation testing of subsea connectors. In: Offshore technology conference, Houston, TX, USA, 1–4 May, OTC-27596
- Ali MH (2018) 42'' Subsea connector & open-PLET technology. In: Offshore technology conference, Houston, TX, USA, 30 April–3 May, OTC-28925
- ASME Boiler and Pressure Vessel Code, VIII Division 2 (2013) Rules for construction of pressure vessels
- Sweeney T, Schnakenburg K (1991) Behavior of 15-ksi subsea wellhead gaskets as determined by analysis and testing. In: Offshore technology conference, Houston, TX, USA, 6–9 May, OTC-6708
- Cao C (2013) Pull-up metal seal system for subsea wellhead equipment. In: International society of offshore and polar engineers, Anchorage, USA, June 30–July 5, ISOPE-1-13-225
- Wang LQ, Wei ZL, Yao SM et al (2015) Performance and optimization of a subsea pipeline mechanical connector. *Chin J Mech Eng* 31(01):142–155
- Zhao HL, Chen R, Luo XL et al (2015) Metal sealing performance of subsea X-tree wellhead connector sealer. *Chin J Mech Eng* 28(3):649–656
- Wei ZL, Wang LQ, Guan Y et al (2016) Static metal sealing mechanism of a subsea pipeline mechanical connector. *Adv Mech Eng* 8(7):1–16
- Yun FH, Wang LQ, Yao SM et al (2017) Analytical and experimental study on sealing contact characteristics of subsea collet connectors. *Adv Mech Eng* 9(4):1–14
- Tang LP, He W, Zhu XH et al (2019) Sealing performance analysis of an end fitting for marine unbounded flexible pipes based on hydraulic-thermal finite element modeling. *Energies* 12:2198
- Carpenter C (2016) Next generation HP/HT subsea wellhead system design challenges and opportunities. In: Society of petroleum engineers, vol 416, pp 73–74
- Gawande SH (2019) Study on the effect of gasket thickness for bolted gearbox flange joint. *SN Appl Sci* 1:32–35
- Haruyama S, Nurhadiyanto D, Choiron MA et al (2013) Influence of surface roughness on leakage of new metal gasket. *Int J Press Vessels Pip* 111–112:146–154
- Beghini M, Bertini L, Santus C et al (2015) Partially open crack model for leakage pressure analysis of bolted metal-to-metal flange. *Eng Fract Mech* 144:16–31
- Korndorf BA (1958) *Hochdrucktechnik in der chemie*. Veb verlag technik, Berlin, pp 15–16
- Bertsch W, Sigel R (1972) The seal problem of high pressure reactor. *Chem Gen Mach* 1(5–6):67–71
- Zhang K, Huang H, Duan ML et al (2017) Theoretical investigation of the compression limits of sealing structures in complex load transferring between subsea connector components. *J Nat Gas Sci Eng* 44:202–213
- Sawa T, Tenma K, Kobayashi T et al (2017) Finite element method stress analysis and evaluation of the sealing performance in box-shape flange gasketed connections subjected to internal pressure. *J Press Vessel Technol* 139(5):051202
- Nash DH, Spence J, Tooth AS et al (2000) A parametric study of metal-to-metal full face taper-hub fanges. *Int J Press Vessels Pip* 77(13):791–797
- Krishna MM, Shunmugam MS, Prasad NS (2007) A study on the sealing performance of bolted flange joints with gaskets using finite element analysis. *Int J Press Vessels Pip* 84:349–357
- Nelson NR, Prasad NS (2016) Sealing behavior of twin gasketed flange joints. *Int J Press Vessels Pip* 138:45–50
- Murtagian GR, Fanelli V, Villasante JA et al (2004) Sealability of stationary metal-to-metal seals. *J Tribol* 126(3):591–596
- Kaculi JT, Witwer BJ (2014) Subsea wellhead system verification analysis and validation testing. In: Offshore technology conference, Houston, TX, USA, 1–4 May, OTC-25163

Publisher's Note Springer Nature remains neutral with regard to jurisdictional claims in published maps and institutional affiliations.